Int J Biomed Comput, 29 (1991) 215–225
Elsevier Scientific Publishers Ireland Ltd.

BUBBLE NUMBER SATURATION CURVE AND ASYMPTOTICS OF HYPOBARIC AND HYPERBARIC EXPOSURES

B.R. WIENKE

Applied Theoretical Physics Division, Los Alamos National Laboratory, Los Alamos, NM 87545 (U.S.A.)

(Received June 28th, 1991)
(Accepted August 24th, 1991)

Within bubble number limits of the varying permeability and reduced gradient bubble models, it is shown that a linear form of the saturation curve for hyperbaric exposures and a nearly constant decompression ratio for hypobaric exposures are simultaneously recovered from the phase volume constraint. Both limits are maintained within a single bubble number saturation curve. A bubble term, varying exponentially with inverse pressure, provides closure. Two constants describe the saturation curve, both linked to seed numbers. Limits of other decompression models are also discussed and contrasted for completeness. It is suggested that the bubble number saturation curve thus provides a consistent link between hypobaric and hyperbaric data, a link not established by earlier decompression models.

Keywords: Bubble models; Asymptotics; Saturation curves; Decompression theory

Introduction

Models [1–20] for controlling and limiting hypobaric and hyperbaric exposures have long differed over range of applicability. Recent testing and comparison of altitude washout data by Conkin and Van Liew [1] question the hypobaric extension of the linear saturation curve, pointing instead to the correlation of altitude data with constant decompression ratio in humans. The analysis of Lanphier and Lehner [2] suggests similar altitude correlations with sheep. Extensions of the saturation curve to altitude have also been discussed by Ingle [3], Bell and Borgwardt [7], Wienke [8], Cross [9], Smith [10], and Bassett [11] in the past, as well as impact on operational diving procedures. On the other hand, correlations [3–6,13,15] of hyperbaric data with a linear saturation curve are well established. Closure of hypobaric and hyperbaric diving data can, however, be effected with a more general form of the saturation curve, one exhibiting the proper behavior in both limits. Just such a curve can be obtained within a model treating both free and dissolved gas buildup and elimination in tissues.

Using the phase volume constraint [16] in a correlated bubble model, [21–23], we

Correspondence to: B.R. Wienke, LANL, MS-F664, Los Alamos, NM 87545, U.S.A.

0020-7101/91/$03.50

have deduced a saturation curve of the form, $M = [\zeta + 1 - \exp(-\xi/P)]P$, for the tissue tensions, M, at absolute pressures, P, and with ζ and ξ bubble constants. In the hypobaric limit, as $P \rightarrow 0$, then $M \rightarrow 0$, while in the hyperbaric limit, as $P \rightarrow \infty$, then $M \rightarrow \zeta P + \xi$. Corresponding tissue ratios, $R = M/P$, are bounded for all pressures. In the hypobaric limit, as $P \rightarrow 0$, then $R \rightarrow \zeta + 1$, while in the hyperbaric limit, as $P \rightarrow \infty$, then $R \rightarrow \zeta$. Thus, a linear form of the saturation curve is recovered for hyperbaric exposures, while a nearly constant decompression ratio is preserved for hypobaric exposures.

Such a general form derives from bubble models, depending crucially on a coupled treatment of both dissolved and free phase gases. Here, we only recount the essential features of the derivation. For convenience, absolute units are employed in analysis, that is, both depth and pressure are measured in feet-of-sea-water (fsw). To convert to nitrogen partial pressure units in tissue quantities such as tension, M, ratio, R, and gradient, G, simple multiplication by the nitrogen mole fraction, 0.79, is appropriate.

Bubble Number and Phase Constraints

Both the varying permeability model [21–23] (VPM) and reduced gradient bubble model [19,20] (RGBM) employ the phase volume constraint [16], but in an integral form. These bubble models assume that the time integrated product of permissible bubble number times supersaturation gradient must remain below some critical limit point, the separated phase volume,

$$\int_{t=0}^{\infty} n\, G\, \mathrm{d}t \leq \omega\, V \tag{1}$$

with n the permissible bubble number, G the supersaturation gradient (difference between supersaturated tissue tension and ambient pressure), t the time, V the separated phase limit, and ω a proportionality constant. Thus, both the bubble number and the supersaturation gradient driving growth are limited by the constraint. This model approach has been applied to both bounce and saturation data [18], and extended to repetitive diving [20], and has proven to be a viable concept in decompression modeling and data correlation.

Experiments [21–23] also suggest that the number density of bubble seeds in aqueous media is exponential in seed radius. The number of bubble seeds excited into growth upon decompression depends directly on bubble radius and inversely on the pressure. Stated another way, bubble excitation radius varies inversely with absolute pressure. Corresponding analyses [18,20] then suggest that the permissible bubble number, n, excited by compression-decompression from absolute pressure, P, back to reference or surface pressure, satisfies the inverse exponential relationship,

$$n = \zeta - \eta \exp(-\xi/P) \tag{2}$$

with ζ, η and ξ bubble constants. The tissue gradient, G, satisfying the phase con-

straint above ultimately takes the form, for saturation exposures,

$$G = [\zeta - \exp(-\xi/P)]P \tag{3}$$

assuming a constant ascent rate, fixed permissible bubble number at saturation, and $\eta = 1$ as the simplest case. The critical gradient, G, or tissue overpressure, certainly approaches zero as ambient pressure approaches zero, and approaches infinity as ambient pressure approaches infinity. By itself, the exponential term approaches zero as ambient pressure approaches zero and one as ambient pressure approaches infinity. Or, for small P, we note,

$$\exp(-\xi/P) \rightarrow 0$$

while, for large P,

$$\exp(-\xi/P) \rightarrow 1 - \xi/P$$

ultimately providing a means to recover the linear representation of the saturation curve for hyperbaric exposures. The corresponding critical tension, M, and critical ratio, R, in the same picture, are given by

$$M = G + P = [\zeta + 1 - \exp(-\xi/P)]P \tag{4}$$

and

$$R = M/P = \zeta + 1 - \exp(-\xi/P) \tag{5}$$

Typical parameter ranges for ξ and ζ, as detailed below, include

$$6.5 \text{ fsw} \leq \xi \leq 14.4 \text{ fsw}$$

$$1.28 \text{ fsw} \leq \zeta \leq 1.45 \text{ fsw}$$

Before considering further analysis of limiting forms, it is first worthwhile to point out that M, G and R are bounded for all values of P, that M and G approach straight lines for large P, bend through the origin for small P, and that R actually varies slightly over P, as implied in the above relationships. Taking a lower bubble surface tension limit of 8.3 fsw, a practical range of absolute pressures for (3), (4) and (5) is

$$5.2 \text{ fsw} \leq P \leq \infty$$

a constraint which has only minimal impact on the asymptotics discussed next.

Bubble Number Saturation Limits and Curves

The expressions given above have relatively simple asymptotic behavior. Limiting

forms appear consistent with fits to the hyperbaric and hypobaric saturation data. In the hypobaric limit of small P, a near constant R is recovered, while in the hyperbaric limit of large P, a linear M is recovered. This can be seen in the following way.

Consider the hypobaric limit first. As $P \rightarrow 0$, then $\exp(-\xi/P) \rightarrow 0$ faster than $P \rightarrow 0$, and therefore,

$$M \rightarrow (\zeta + 1)P$$

$$G \rightarrow \zeta P$$

$$R \rightarrow \zeta + 1$$

Quite obviously, M and G approach zero, while R remains nearly constant, in this limit. But, in the hyperbaric limit, as $P \rightarrow \infty$, then $\exp(-\xi/P) \rightarrow 1 - \xi/P$ at roughly the same rate as P, so that

$$M \rightarrow (\zeta + 1 - 1 + \xi/P)P \rightarrow \zeta P + \xi$$

$$G \rightarrow (\zeta - 1 + \xi/P)P \rightarrow (\zeta - 1)P + \xi$$

$$R \rightarrow \zeta$$

At this limit, M and G increase linearly with pressure, and R remains nearly constant.

Turning to estimation of ξ and ζ, there are reference points at the two pressure extremes. For comparison of parameter ranges, it is instructive to first estimate ξ and ζ over hyperbaric and hypobaric data, each individually, and then estimate ξ and ζ over both regions. Sea-level pressure, $P = 33$ fsw, serves to separate the two regions. The range of ξ and ζ, over the three cases, is seen to be compact as follows.

Hyperbaric estimation of ξ and ζ

Air saturation data for hyperbaric exposures is plentiful, with important parameterizations of M as a function of P discussed shortly. Taking permissible tensions, $M = 54, 97, 140$ fsw at absolute pressures, $P = 33, 66, 99$ fsw, we obtain

$$\xi = 14.4 \text{ fsw}$$

$$\zeta = 1.28$$

Hypobaric estimation of ξ and ζ

Following Conkin and Van Liew [1] in suggesting an aerial bends threshold at 13 000 ft, that is, $M = 33$ fsw at $P = 20$ fsw, and also taking critical tensions, $M = 13.5, 54$ fsw at absolute pressures, $P = 5.2, 33$ fsw yields

$$\xi = 6.55 \text{ fsw}$$

$$\zeta = 1.45$$

Hyperbaric-hypobaric estimation of ξ and ζ

Including all five data points from both of the above cases, we find

$$\xi = 11.27 \text{ fsw}$$

$$\zeta = 1.31$$

This parametrization weighs both hypobaric and hyperbaric data equally. In principle, ξ and ζ could be fitted to any set of exposure data.

Fits in the hypobaric, hyperbaric and hypobaric-hyperbaric regimes exhibit consistency in ξ and ζ corroborating the functional form of the curve. Figures 1, 2 and 3 depict tissue M, G and R over pressure range, 5.2 fsw $\leq P \leq$ 66 fsw, employing Eqns. (3), (4) and (5), taking $\xi = 11.27$ fsw and $\zeta = 1.31$. The asymptotic behavior described above is clearly visible, that is, linear M and G for large P, exponential dropoff of M and G through the origin for small P, and slight variation of R over P.

Other Model Comparisons

Saturation curves for various models exhibit different forms in the large and small ambient pressure limits. Employing absolute units of pressure and depth in fsw, denoting critical tissue tensions, M, critical gradients, G, and critical decompression

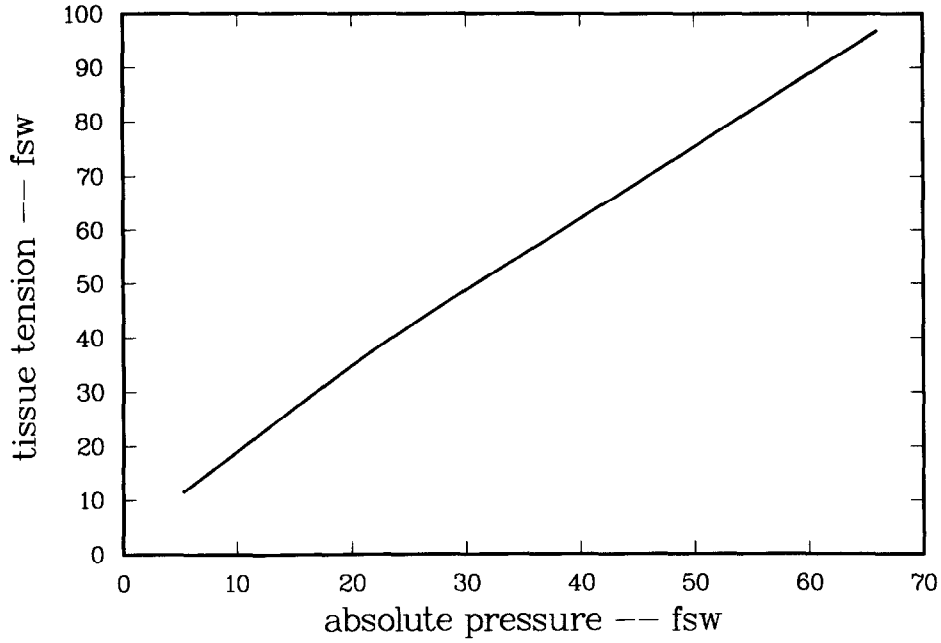

Fig. 1. Bubble number saturation curve for tissue tensions. The permissible tissue tension, M, satisfies the relationship (fsw), $M = [2.31 - \exp(-11.3/P)]P$, for P, the pressure. Pressure units are absolute. For large P the curve approaches a straight line, while for small P the curve falls off rapidly, passing through the origin.

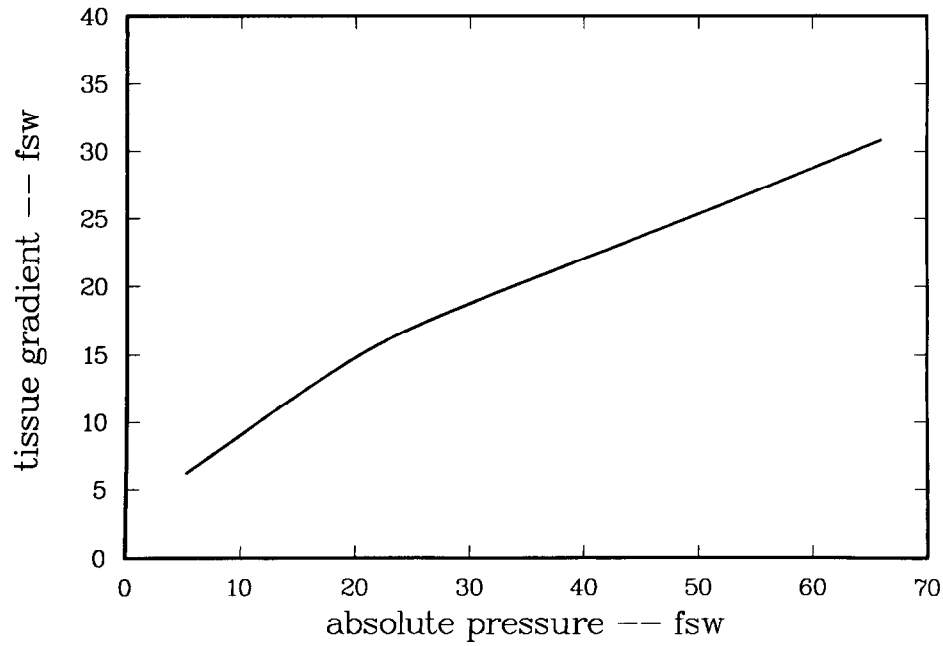

Fig. 2. Bubble number saturation curve for tissue gradients. In analogy with the tension, the tissue gradient, G, exhibits similar asymptotic behavior. The permissible gradient, G, satisfies (fsw), $G = [1.31 - \exp(-11.3/P)]P$, approximating a straight line for large P, and curving through the origin as P becomes small. Pressure units are absolute.

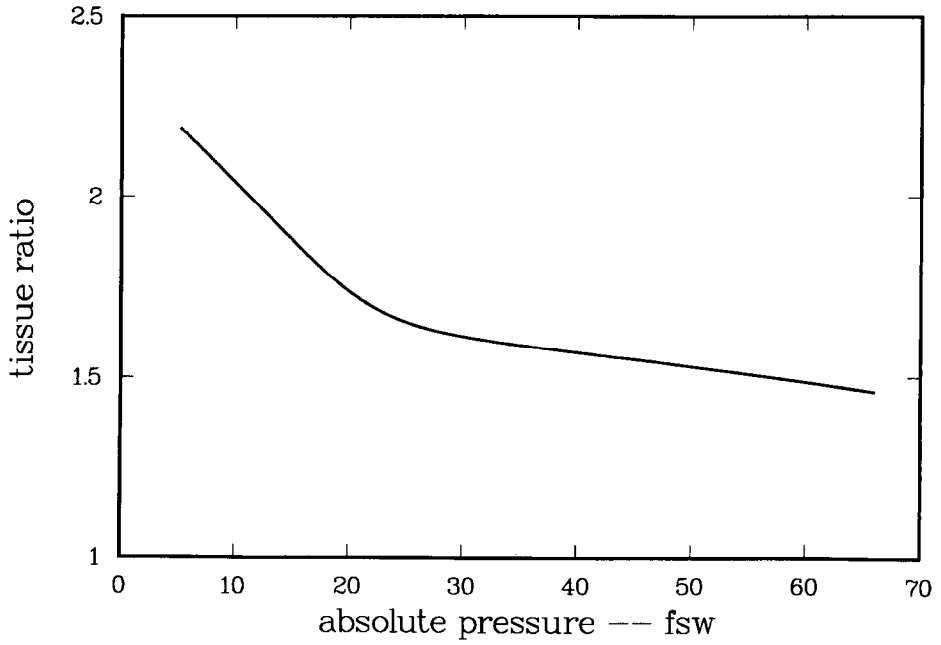

Fig. 3. Bubble number saturation curve for tissue ratios. The tissue ratio, R, approaches a constant value in both the large and small P limit, $R = 2.31 - \exp(-11.3/P)$, that is, 2.31 for small P and 1.31 for large P, with pressure units (fsw) absolute as before.

ratios, R, at absolute pressure, P, with $G = M - P$ and $R = M/P$, as before, it is illuminating to compare other models at opposite pressure extremes. Again, to convert to nitrogen partial pressure units, appropriate tissue pressures are multiplied by 0.79.

Haldane fixed ratio limits

Haldane's early experiments with goats suggest a fixed decompression ratio, that is, the critical ratio of tissue tension to ambient pressure in all compartments. The classical [3] saturation curve is thus linear with zero intercept, given by

$$M = \chi P \tag{6}$$

or equivalently,

$$G = (\chi - 1)P \tag{7}$$

$$R = \chi \tag{8}$$

Ranges of χ include

$$1.5 \leq \chi \leq 3.5$$

According to Haldane, $\chi = 2$, of course, but other values have been employed in diving applications.

The hypobaric limit is simple. As $P \to 0$, then $M \to 0$, $G \to 0$ and $R = \chi$. All critical parameters are thus bounded in the fixed ratio model. The hyperbaric limit, as $P \to \infty$, requires $M \to \chi P$, $G \to (\chi - 1)P$ and $R = \chi$.

Multi-tissue tension limits

When extending the Haldane model to broader classes of exposures, critical tensions vary across tissue compartments, with the slowest tissue controlling saturation exposures. The multi-tissue [4–8] extension of the classical saturation curve is also linear, but with non-zero intercept, according to

$$M = \alpha P + \beta \tag{9}$$

or

$$G = (\alpha - 1)P + \beta \tag{10}$$

$$R = \alpha + \beta/P \tag{11}$$

Typical ranges of α and β in the slow compartments, $120 \leq \tau \leq 720$ min, are

$$1.30 \leq \alpha \leq 1.40$$

$$11.1 \text{ fsw} \leq \beta \leq 17.1 \text{ fsw}$$

Corresponding limits, as $P \rightarrow 0$, require $M \rightarrow \beta$, $G \rightarrow \beta$ and $R \rightarrow \infty$. The ratio, R, is thus not bounded for hypobaric exposures in the multi-tissue model. At increasing pressure, as $P \rightarrow \infty$, then $M \rightarrow \alpha P$, $G \rightarrow (\alpha - 1)P$, while $R \rightarrow \alpha$. The hyperbaric behavior of the multi-tissue model parallels the fixed ratio model, but with different parameter values.

Altitude similarity limits

Holding the sea-level decompression ratios constant at altitude induces an exponential scaling of critical tensions and gradients, rendering altitude excursions similar to hyperbaric exposures. The similarity [8–11] saturation curve is linear-exponential with zero intercept, that is, it is broken up into two pieces. For $P > 33$ fsw,

$$M = \alpha P + \beta \tag{12}$$

with

$$G = (\alpha - 1)P + \beta \tag{13}$$

$$R = \alpha + \beta/P \tag{14}$$

while, for $P \leq 33$ fsw, and with convenient parameterization, $P = 33 \exp(-\gamma z)$ for $\gamma = 0.0000385$ ft^{-1} and z the elevation in feet,

$$M = [33\alpha + \beta] \exp(-\gamma z) \tag{15}$$

and

$$G = [33(\alpha - 1) + \beta] \exp(-\gamma z) \tag{16}$$

$$R = \alpha + \beta/33 \tag{17}$$

Again,

$$1.30 \leq \alpha \leq 1.40$$

$$11.1 \text{ fsw} \leq \beta \leq 17.1 \text{ fsw}$$

as noted in the multi-tissue model.

But, unlike the multi-tissue limits, as $z \rightarrow \infty$, then certainly $P = 33 \exp(-\gamma z) \rightarrow 0$, and $M \rightarrow 0$, $G \rightarrow 0$, but $R = \alpha + \beta/33$. The similarity approach is also a fixed ratio at altitude, and thus bounded. In the hyperbaric limit, the similarity model approaches the same limits as the multi-tissue model.

Fixed gradient limits

A fixed gradient serves as an alternative to a fixed ratio in single tissue models. The fixed gradient [8,12,13] saturation curve is thus linear with non-zero intercept,

$$M = \delta + P \tag{18}$$

or

$$G = \delta \tag{19}$$

$$R = 1 + \delta/P \tag{20}$$

The single gradient parameter, δ, ranges in applications,

$$18 \text{ fsw} \leq \delta \leq 28 \text{ fsw}$$

As $P \to 0$, then $M \to \delta$, $G = \delta$, while $R \to \infty$. As in the multi-tissue case, the ratio is not bounded for hypobaric exposures in the fixed gradient model. In the hyperbaric limit, as $P \to \infty$, then $M \to P$, $G = \delta$, but $R \to 1$.

Variable ratio limits

Because the fixed gradient is often conservative for deep exposures and liberal for shallow exposures, a variable decompression ratio, depending on depth, is employed in diffusion models. Accordingly, the variable ratio [8,13,15] saturation curve is bilinear with zero intercept, that is,

$$M = \frac{\upsilon P}{P + \mu} \tag{21}$$

with

$$G = \left[\frac{\upsilon}{P + \mu} - 1\right] P \tag{22}$$

$$R = \frac{\upsilon}{P + \mu} \tag{23}$$

The variable rates parameters, υ and μ, have typical hyperbaric values,

$$890 \text{ fsw} \leq \upsilon \leq 910 \text{ fsw}$$

$$395 \text{ fsw} \leq \mu \leq 410 \text{ fsw}$$

The hypobaric limits, as $P \to 0$, are $M \to 0$, $G \to 0$, and $R \to \upsilon/\mu$. In the variable ratio model, all critical parameters are well behaved and bounded at reduced pressure. However, in the hyperbaric limit, as $P \to \infty$, then $M \to \upsilon$, $G \to -P$ and $R \to 0$. Thus at increasing pressure, the variable ratio model becomes unphysical.

Separated phase volume limits

In the thermodynamic model, the separated phase volume serves as the bends trigger point, linked to perfusion-diffusion gas exchange and tissue bulk modulus. The

phase volume [14–16] saturation curve is similarly linear with non-zero intercept,

$$M = \kappa P + \lambda \tag{24}$$

with

$$G = (\kappa - 1)P + \lambda \tag{25}$$

$$R = \kappa + \lambda/P \tag{26}$$

The phase volume parameters, κ and λ, range

$$1.36 \leq \kappa \leq 1.60$$

$$7.5 \text{ fsw} \leq \lambda \leq 13.1 \text{ fsw}$$

Still, as $P \rightarrow 0$, limits parallel the multi-tissue case, that is, $M \rightarrow \lambda$, $G \rightarrow \lambda$ and $R \rightarrow \infty$. The ratio, as with other linear tension models, is not bounded for hypobaric exposures. In the hyperbaric case, as $P \rightarrow \infty$, then $M \rightarrow \kappa P$, $G \rightarrow (\kappa - 1)P$ and $R \rightarrow \kappa$.

To compare models and constants, it is useful to normalize curves to the same exposures in terms of basic parameters. Accordingly, taking the less conservative gradients, $G = 16.5$, 21 fsw at sea-level and at 18 000 ft elevation, that is, $P = 16.5$, 33 fsw, appropriate values of all constants can be generated. Corresponding tissue tensions and ratios similarly take the values, $M = 33$, 54 fsw and $R = 2.00$, 1.63. Accordingly, we find,

$$\chi \approx 1.64$$

$$\alpha = \kappa \approx 1.27$$

$$\beta = \lambda \approx 12 \text{ fsw}$$

$$\delta \approx 21 \text{ fsw}$$

$$\upsilon \approx 148.50 \text{ fsw}$$

$$\mu \approx 57.75 \text{ fsw}$$

$$\zeta \approx 1.40$$

$$\xi \approx 12.0 \text{ fsw}$$

as a normalized set for model comparisons.

Conclusions

The varying permeability and reduced gradient bubble models, coupling dissolved and free gas buildup and elimination to the phase volume constraint, suggest saturation curves asymptotically consistent with both hypobaric and hyperbaric exposure

data. Two bubble constants, related to seed number density and permissible excess, parameterize hypobaric and hyperbaric data well. Such closure on first principle has not been seen in previous decompression models and algorithms. It is thus hoped that these saturation curves provide a useful departure point for computational decompression modeling. Such a simple set of saturation relationships, specifically Eqns. (3), (4) and (5), can easily be applied or fitted to any set of exposure data.

References

1 Conkin J and Van Liew HD: Failure of the straight-line boundary between safe and unsafe decompressions when extrapolated to the hypobaric realm, *Undersea Biomed Res*, 18 (1991) 16.
2 Sheffield PJ: *Flying After Diving*, Undersea and Hyperbaric Medical Society Publication, UHMS 77 (FLYDIV), Bethesda, 1989.
3 Boycott AE, Damant GCC and Haldane JS: The prevention of compressed-air illness, *J Hyg*, 8 (1908) 342–443.
4 Buhlmann AA: *Decompresssion/Decompression Sickness*, Springer-Verlag, Berlin, 1984.
5 Workman RD: Calculation of decompression schedules for nitrogen-oxygen and helium-oxygen dives, USN Experimental Diving Unit Research Report, NEDU 6–65, Washington, DC, 1965.
6 Spencer MP: Decompression limits for compressed air determined by ultrasonically detected blood bubbles, *J Appl Physiol*, 40 (1976) 229–235.
7 Bell RL and Borgwardt RE: The theory of high altitude correction to the US Navy Standard Decompression Tables: I. The cross corrections, *Undersea Biomed Res*, 3 (1976) 1–23.
8 Wienke BR: Tissue gas exchange models and decompression computations: a review, *Undersea Biomed Res*, 16 (1989) 53–89.
9 Cross ER: High altitude decompression, *Skin Diver Mag*, 19 (1970) 17–18.
10 Smith CL: *Altitude Procedures for the Ocean Diver*, NAUI Publication Number 5, Colton, 1976.
11 Bassett BE: And yet another approach to the problems of altitude diving and flying after diving, *Proc. Decompression in Depth*, PADI, Santa Ana, 1979.
12 Hill L and McLeod JJ: The influence of compressed air on respiratory exchange, *J Physiol*, 29 (1903) 492–510.
13 Bennett PB and Elliott DH: *The Physiology and Medicine of Diving and Compressed Air Work*, Bailliere, Tindall and Cassell, London, 1969.
14 LeMessurier DH and Hills BA: Decompression sickness: a study of diving techniques in the Torres Strait, *Hvaldradets Skrifter*, 48 (1965) 54–84.
15 Hills BA: *Decompression Sickness*, Wiley, New York, 1977.
16 Hennessy TR and Hempleman HV, An examination of the critical released gas concept in decompression sickness, *Proc R Soc London B*, 197 (1977) 299–313.
17 Yount DE and Strauss RH: Bubble formation in gelatin: a model for decompression sickness, *J Appl Phys*, 47 (1976) 5081–5089.
18 Yount DE and Hoffman DC: On the use of a bubble formation model to calculate diving tables, *Aviat Space Environ Med*, 57 (1986) 149–156.
19 Wienke BR, Modeling dissolved and free phase gas dynamics under decompression, *Int J Biomed Comput*, 30 (1990) 112–118.
20 Wienke BR: Reduced gradient bubble model, *Int J Biomed Comput*, 26 (1990) 237–256.
21 Yount DE, On the evolution, generation, and regeneration of gas cavitation nuclei, *J Acoust Soc Am*, 71 (1982) 1473–1481.
22 Yount DE, Skins of varying permeability: a stabilization mechanism for gas cavitation nuclei, *J Acoust Soc Am*, 65 (1979) 1431–1439.
23 Yount DE, Yeung CM and Ingle FW: Determination of the radii of gas cavitation nuclei by filtering gelatin, *J Acoust Soc Am*, 65 (1979) 1440–1450.